

Stabilization of Co^{2+} in layered double hydroxides (LDHs) by microwave-assisted ageing

M. Herrero, P. Benito, F.M. Labajos, V. Rives*

Departamento de Química Inorgánica, Universidad de Salamanca, Salamanca-37008, Spain

Received 6 October 2006; received in revised form 29 November 2006; accepted 11 December 2006

Available online 15 December 2006

Abstract

Co-containing layered double hydroxides at different pH have been prepared, and aged following different routes. The solids prepared have been characterized by element chemical analysis, powder X-ray diffraction, thermogravimetric and differential thermal analyses (both in nitrogen and in oxygen), FT-IR and Vis-UV spectroscopies, temperature-programmed reduction and surface area assessment by nitrogen adsorption at -196°C . The best conditions found to preserve the cobalt species in the divalent oxidation state are preparing the samples at controlled pH, and then submit them to ageing under microwave irradiation.

© 2006 Elsevier Inc. All rights reserved.

Keywords: Hydrotalcite; Microwave; Layered double hydroxides; Cobalt

1. Introduction

Layered double hydroxides (LDHs) consist of brucite-like layers where a partial divalent/trivalent cations has taken place, resulting in positively charged layers, balanced by anions between the brucite-like layers; compounds with this structure where monovalent and tetravalent ones isomorphically substitute the divalent and trivalent cations are also known [1–3]. This results in a 3R ordered stacked polytype for synthetic materials [4], wherein anions and water molecules are located in the interlamellar region. A wide range of anions balancing the positive charge in excess in the layers (because of the M(II)/M(III) substitution) have been reported [5,6], and the nature of the cations in the layers can be also varied in a wide range, the main limitation being their ionic size. They are also commonly known as “hydrotalcites” or “hydrotalcite-like” materials, after the mineral hydrotalcite $[\text{Mg}_6\text{Al}_2(\text{OH})_{16}][(\text{CO}_3) \cdot 4\text{H}_2\text{O}]$.

Cobalt-containing hydrotalcites have been used for several applications; they have been used as precursors to prepare Fischer–Trops catalysts [7,8], and are active in

catalytic decomposition of N_2O [9–13], selective conversion of acetone [14], removal of SO_2 and NO_x [15], steam reforming of methanol [16], and hydroxylation of phenol [17,18]. The selectivity and conversion of these catalysts depend on the method followed to prepare them, cobalt concentration and ageing process they have submitted to [19]. Calcination of hydrotalcites, on the other hand, leads to well-dispersed mixed oxides, which find also application in several catalytic processes. For these reasons, a large number of cobalt hydrotalcites have been prepared where cobalt replaces completely to the divalent cation, e. g., Co,Al-LDHs [20–22] and Co,Cr or Co,Fe hydrotalcites [23–25]. Xu and Zeng [26–28] have synthesized monometallic cobalt hydrotalcites in order to obtain Co_3O_4 spinels, without rising the temperature to the levels generally needed, by in situ cobalt oxidation to the trivalent state.

When cobalt hydrotalcites are submitted to thermal ageing treatments such as hydrothermal treatment, Ullbarri et al. [21] noticed that part of the divalent cobalt is oxidized to the trivalent state, probably due to the easy formation of the cobalt spinel, Co_3O_4 . Leroux et al. [29] have also reported that the oxidation rate depends on the Co/Al ratio, Co^{3+} existing in the structure when such a ratio is equal or larger than 5. The oxidation process

*Corresponding author. Fax: +34 923 29 45 74.

E-mail address: vrives@usal.es (V. Rives).

induces structural changes in the solid, and part of the trivalent aluminium migrates to the interlamellar region. Moreover, as a result of the oxidation process, a higher net charge is also developed and new carbonate anions are needed in the interlayer to balance the charge in excess.

Monometallic hydrotalcite-like compounds containing Co(II)–Co(III) were synthesized by precipitation followed by microwave irradiation during the hydrothermal treatment step [30]; however, only a poorly crystallized hydrotalcite was detected after 1 min irradiation time, and on increasing the irradiation time the hydrotalcite network was destroyed. In this work, we have also applied the advantages linked to the microwave heating [31]—rapid heating, smaller thermal gradient, environmental friendly, and cheaper than the conventional ageing process of cobalt hydrotalcites—to prepare well-crystallized compounds, but avoiding the oxidation process. For these purposes, several series of hydrotalcites have been prepared modifying the pH of the synthesis and ageing temperature.

2. Experimental

2.1. Synthesis of the solids

All samples were prepared by the coprecipitation method described by Reichle [32]. The chemicals, $\text{Co}(\text{NO}_3)_2 \cdot 6\text{H}_2\text{O}$, $\text{Al}(\text{NO}_3)_3 \cdot 9\text{H}_2\text{O}$, NaOH, and Na_2CO_3 , were purchased from Fluka and were used without any further treatment. The nominal Co/Al ratio was in all cases 2/1. The pH of the synthesis was modified on purpose to study its effect in the Co(II) oxidation process. A series of samples (hereafter bCA) were prepared at unfixed pH by addition of an excess of base to the initial solution; on the contrary, for samples belonging to the aCA system the pH was kept at a constant value of 9 during synthesis by addition of a 1 M NaOH solution from a 240 Crison pH-burette. The slurry prepared in both cases was submitted to different ageing treatments: (i) conventional hydrothermal treatment for 1 day at 100 °C in a stainless-steel Phaxe 2000 bomb lined with Teflon; (ii) microwave-hydrothermal treatment for different periods of time (10, 30, 60 and 180 min) at 100 and 125 °C; a portion of sample was also stored without any ageing treatment. The microwave-hydrothermal experiments were carried out in a MILESTONE ETHOS PLUS microwave oven where reactants were treated in Teflon liners. The microwave oven uses 2.45 GHz frequency and the power supplied was that necessary to attain the temperature previously programmed, which was measured by a thermocouple. The precipitates were separated and washed by centrifugation with distilled water until complete removal of charge balancing anions and cations in the starting salts and dried at 40 °C in a furnace.

The samples were named, Table 1, depending on the hydrothermal treatment they had been submitted to: a/b-CA0 for the fresh samples, i.e. not aged, a/b-CAC for those aged by the conventional hydrothermal treatment,

Table 1
Labelling of the samples studied

Sample	Thermal treatment	pH
a-CA0	No treatment	9
a-CAC	Convective treatment	9
a-1CA t^a	MW ^b -treatment 100 °C	9
a-CA t	MW-treatment 125 °C	9
b-CA0	No treatment	Unfixed
b-CAC	Convective treatment	Unfixed
b-1CA t	MW-treatment 100 °C	Unfixed
b-CA t	MW-treatment 125 °C	Unfixed

^a $t = 10, 30, 60$ or 180 min.

^bMW = microwave.

a/b-1CA t for the samples treated in the microwave oven at 100 °C and a/b-CA t when the microwave temperature was 125 °C. In these cases, t means the irradiation time in min ($t = 10, 30, 60, 180$ and 300 min). As no important difference was found for the samples treated for 300 min with respect to those treated for 180 min, most of the results here reported will be limited to samples treated up to 180 min under hydrothermal-microwave conditions.

2.2. Techniques

Element chemical analyses for Co and Al were carried out by atomic absorption in a Mark 2 ELL-240 apparatus, in Servicio General de Análisis Químico Aplicado (University of Salamanca, Spain).

Powder X-ray diffraction (PXRD) patterns were recorded in a Siemens D-500 instrument using Cu- $K\alpha$ radiation ($\lambda = 1.54050 \text{ \AA}$) and equipped with Diffrac AT software. Identification of the crystalline phases was made by comparison with the JCPDS files [33].

UV–Vis spectra were recorded following the diffuse reflectance (UV–Vis/DR) technique in a Perkin-Elmer Lambda 35 instrument with a Labsphere RSA-PE-20 integrating sphere and software UV WinLab, using 2 nm slits and MgO as reference.

Thermogravimetric (TG) and differential thermal analyses (DTA) were carried out in TG-7 and DTA-7 instruments from Perkin-Elmer, in flowing oxygen and/or nitrogen (from L'Air Liquide, Spain), at a heating rate of 10 °C min⁻¹.

FT-IR spectra were recorded in a Perkin-Elmer FT1730 instrument, using KBr pellets; 100 spectra (recorded with a nominal resolution of 4 cm⁻¹) were averaged to improve the signal-to-noise ratio.

Temperature-programmed reduction (TPR) analyses were carried out in a Micromeritics 2900 TPD/TPR instrument. The reducing agent was H₂/Ar (5% vol) from L' Air Liquide (Spain) and the gas flow (50 ml min⁻¹), sample weight (15–20 mg), and heating schedule (10 °C min⁻¹) were chosen according to the literature [34] to optimize resolution of the curves. Calibration of the instrument was carried out with CuO (from Merck).

Specific surface assessment was carried out in a Gemini instrument from Micromeritics. The sample (ca. 80–100 mg) was previously degassed in flowing nitrogen at 110 °C for 2 h in a FlowPrep 060 apparatus, also from Micromeritics, in order to remove physisorbed water, and the data were analysed using published software [35].

3. Results

3.1. Element chemical analyses

The results obtained are summarized in Tables 2 and 3, together with the formulae calculated for the samples; the water content has been determined from the TG studies (see below). The carbonate content was calculated from Co/Al atomic ratios, assuming carbonate is the only charge-balancing interlayer anion. The experimental M^{2+}/M^{3+} values are 15–30% larger than the expected (nominal) ones; such a deviation is especially significant for

those samples prepared at high pH, probably because under these conditions aluminium ions become partially dissolved as aluminate species. Nevertheless, this effect is not very uncommon, and deviations from nominal ratios have been generally ascribed to a preferential dissolution or precipitation of the divalent or the trivalent cations [36]. No significant change in the chemical composition is observed for the samples submitted to hydrothermal treatments, with or without microwave irradiation.

3.2. Powder X-ray diffraction (PXRD)

Selected PXRD patterns are shown in Fig. 1. All they are characteristic of the hydrocalcite-like structure (no other crystalline phase was identified), with rather sharp peaks due to diffraction by basal planes, recorded below $2\theta = 30^\circ$. However, a detailed analysis of the peaks recorded in the middle range of the diagram (peaks due to diffraction by non-basal planes, involving the interlayer

Table 2

Element chemical analysis data for Co and Al (weight percentage), Co/Al molar ratio, synthesis conditions (pH control, temperature of hydrothermal treatment), formula of the fresh solids and those aged by the conventional hydrothermal treatment, lattice parameters (c , a , in Å) and average particle size from X-ray diffraction lines broadening (D , in Å)

Sample	Co ^a	Al ^a	Co/Al ^b	Temperature ^c	pH control	Formula	c	a	D
a-CA0	34.76	6.62	2.41	25	Yes	[Co _{0.71} Al _{0.29} (OH) ₂] (CO ₃) _{0.145} · 0.91H ₂ O	23.0	3.068	80
a-CAC	35.61	7.09	2.30	100	Yes	[Co _{0.70} Al _{0.30} (OH) ₂] (CO ₃) _{0.150} · 0.80H ₂ O	23.0	3.078	380
b-CA0	35.14	7.05	2.28	25	No	[[Co _{0.70} Al _{0.30} (OH) ₂] (CO ₃) _{0.150} · 0.90H ₂ O	22.7	3.068	130
b-CAC	37.30	6.62	2.58	100	No	[Co _{0.72} Al _{0.28} (OH) ₂] (CO ₃) _{0.140} · 0.64H ₂ O	22.7	3.070	400

^aWeight percentage.

^bMolar ratio.

^c°C.

Table 3

Element chemical analysis data for Co and Al (weight percentage), Co/Al molar ratio, synthesis conditions (pH control, temperature of hydrothermal treatment), formula of the solids aged by the microwave hydrothermal treatment, lattice parameters (c , a , in Å) and average particle size from X-ray diffraction lines broadening (D , in Å)

Sample	Co ^a	Al ^a	Co/Al ^b	Temperature ^c	pH control	Formula	c	a	D
a-1CA10	35.00	7.04	2.28	100	Yes	[Co _{0.69} Al _{0.31} (OH) ₂] (CO ₃) _{0.155} · 0.79H ₂ O	22.9	3.072	130
a-1CA30	34.50	6.94	2.28	100	Yes	[Co _{0.69} Al _{0.31} (OH) ₂] (CO ₃) _{0.155} · 0.72H ₂ O	22.7	3.066	130
a-1CA60	37.48	7.06	2.43	100	Yes	[Co _{0.71} Al _{0.29} (OH) ₂] · (CO ₃) _{0.145} · 0.71H ₂ O	23.0	3.072	140
a-1CA180	35.70	7.18	2.28	100	Yes	[Co _{0.69} Al _{0.31} (OH) ₂] (CO ₃) _{0.155} · 0.61H ₂ O	22.6	3.064	180
a-CA10	37.52	7.32	2.23	125	Yes	[Co _{0.69} Al _{0.31} (OH) ₂] (CO ₃) _{0.155} · 0.66H ₂ O	22.7	3.070	150
a-CA30	36.00	6.88	2.40	125	Yes	[Co _{0.71} Al _{0.29} (OH) ₂] (CO ₃) _{0.145} · 0.65H ₂ O	22.6	3.066	190
a-CA60	38.30	7.00	2.51	125	Yes	[Co _{0.71} Al _{0.29} (OH) ₂] (CO ₃) _{0.145} · 0.62H ₂ O	23.0	3.076	250
a-CA180	38.48	7.58	2.32	125	Yes	[Co _{0.70} Al _{0.30} (OH) ₂] (CO ₃) _{0.150} · 0.64H ₂ O	22.6	3.066	290
b-1CA10	36.76	6.52	2.58	100	No	[Co _{0.72} Al _{0.28} (OH) ₂] (CO ₃) _{0.140} · 1.05H ₂ O	22.7	3.068	170
b-1CA30	35.85	6.42	2.56	100	No	[Co _{0.72} Al _{0.28} (OH) ₂] (CO ₃) _{0.140} · 0.75H ₂ O	22.9	3.074	210
b-1CA60	36.88	6.78	2.49	100	No	[Co _{0.71} Al _{0.29} (OH) ₂] (CO ₃) _{0.145} · 0.76H ₂ O	22.8	3.068	390
b-1CA180	33.68	6.04	2.55	100	No	[Co _{0.72} Al _{0.28} (OH) ₂] (CO ₃) _{0.140} · 0.73H ₂ O	23.0	3.076	210
b-CA10	36.48	6.44	2.59	125	No	[Co _{0.72} Al _{0.28} (OH) ₂] (CO ₃) _{0.140} · 0.71H ₂ O	22.6	3.064	240
b-CA30	38.00	7.02	2.48	125	No	[Co _{0.71} Al _{0.29} (OH) ₂] (CO ₃) _{0.145} · 0.69H ₂ O	23.1	3.080	410
b-CA60	36.72	6.62	2.54	125	No	[Co _{0.72} Al _{0.28} (OH) ₂] (CO ₃) _{0.140} · 0.83H ₂ O	22.8	3.070	300
b-CA180	36.20	6.26	2.65	125	No	[Co _{0.73} Al _{0.27} (OH) ₂] (CO ₃) _{0.135} · 0.71H ₂ O	23.0	3.080	270

^aWeight percentage.

^bMolar ratio.

^c°C.

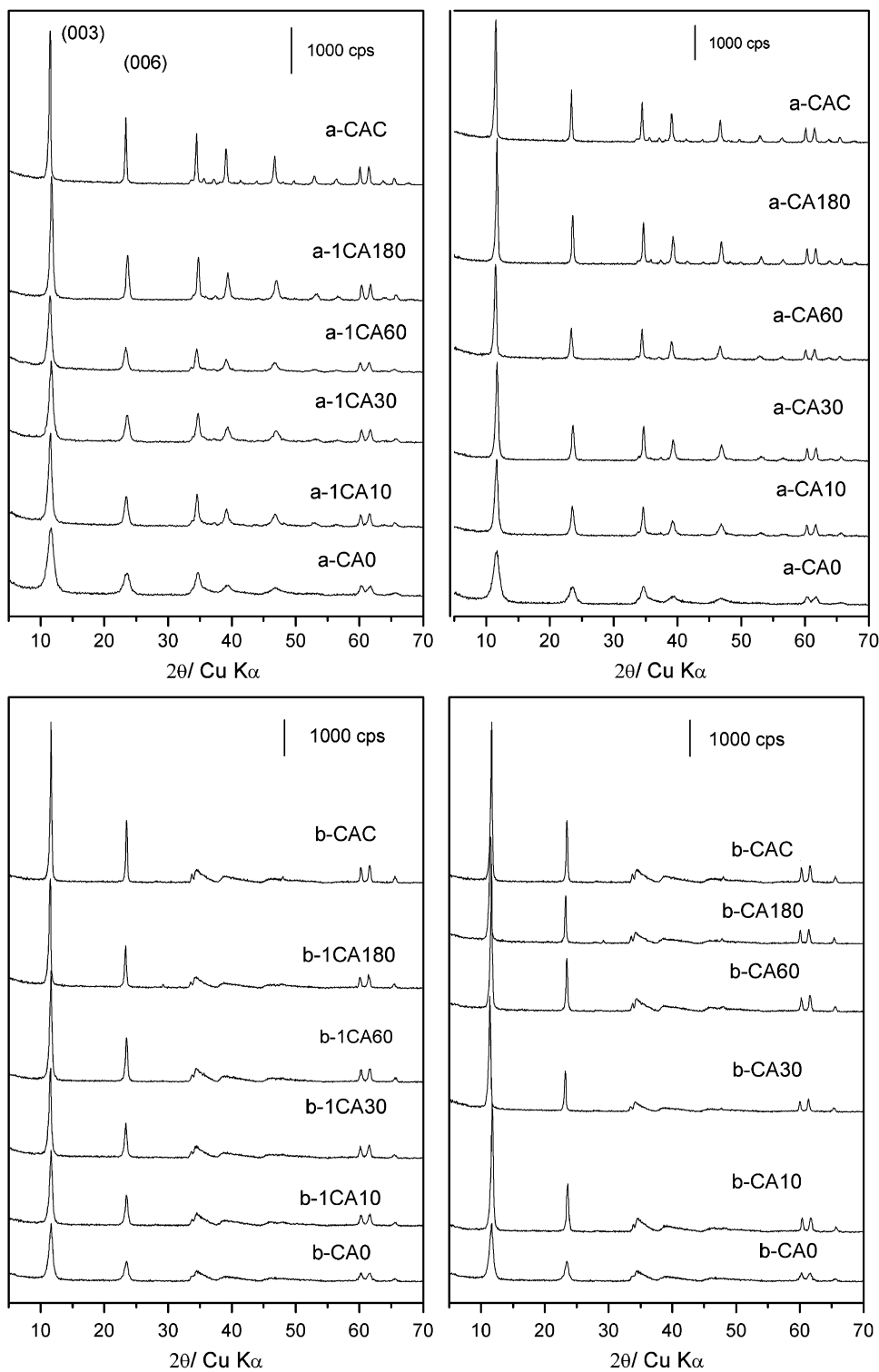


Fig. 1. X-ray powder diffraction patterns of the samples studied. Above: system a-CA. Bottom: system b-CA. The patterns have been vertically displaced for clarity.

species, are recorded in this angle range) shows some important differences. For samples belonging to series “b”, prepared at high, uncontrolled pH, these peaks are rather broad and asymmetric, while for samples “a”, prepared at pH = 9, these peaks are more symmetric, as those due to basal reflections are. This means that at pH = 9, the

turbostratic disorder is diminished and a better ordered stacking of the layers is attained. It should be stressed that such a behaviour should be related to the pH during precipitation and not to the use of microwave radiation, as it is observed also for the unaged sample and for that aged under conventional conditions.

The only phase recorded is hydrotalcite; Co_3O_4 crystal-line spinel phase, whose presence has been previously reported when the slurry was heated under microwave radiation [30], is not detected. There are appreciable differences between the PXRD patterns of the samples before and after microwave-hydrothermal and conventional hydrothermal treatment. At first sight, an enhancement in sample crystallinity (related to sharpness of the diffraction peaks) with increasing the irradiation time is observed. With respect to the irradiation temperature, the enhancement is more remarkable at 125°C (Samples a-CA t y b-CA t) than at 100°C (Samples a-1CA t y b-1CA t), but both temperatures lead to well-crystallized materials. It should be noticed that some anomalous behaviours are detected; in samples belonging to series a synthesized at $\text{pH} = 9$ (series a-CA), although the initial heating for 10 min under microwave irradiation, sample a-1CA10, leads to an improvement in the crystalline order, there are no differences between samples treated for 30 and 60 min, samples a-1CA30 and a-1CA60. Moreover, for samples prepared at high pH and aged at 100°C (series b-1CA), the maximum sharpness of the diffraction peaks is reached after 60 min microwave irradiation, sample b-1CA60, and when the irradiation time is further increased at 100°C the crystallinity decreases, while at 125°C a non-well-defined trend is observed. The weakening of the PXRD peak intensity might suggest a structural degradation of the LDHs after the prolonged ageing [37], although the patterns do not evidence Co_3O_4 formation. Another feature to be considered is the change in the relative intensity of the (110) and (113) reflections, the doublet recorded close to $2\theta = 60^\circ$, during the treatment.

In order to obtain more information about the crystallinity of the samples, the crystallite size was calculated by applying the Debye–Scherrer equation, from the full-width at half-maximum (FWHM) intensity of the (003) diffraction peaks. The Warren correction was used for instrumental line broadening, while the possible contribution of the disorder effect and/or lattice strains was ignored [38]. The calculated values are included in Tables 2 and 3 for both series of samples. The values reported confirm the enhancement of the crystallinity of the compounds when the irradiation time is increased. For example, the crystallite size varies from 80 Å for the non-treated sample to 290 Å for the sample irradiated for 180 min at 125°C , a-CA180.

The cell parameters have been calculated assuming a 3R polytype [4], and they are quite similar to those obtained for other hydrotalcite-like compounds containing carbonate as the interlayer anion. No significant differences in the lattice parameters are observed from one sample to another. Lattice parameter a corresponds to the average cation–cation distance within a given layer, while parameter c corresponds to three times the thickness of an elemental “sandwich”. The first parameter depends mostly on the ionic radii of the layer cations, while the second one

depends on the size of the interlayer anion and on its orientation in the interlayer (in the case of non-spherical anions), as well as on the electrostatic interaction between the interlayer species and the layers; as the chemical composition is so similar for all samples prepared, the lattice parameters measured for all samples prepared are very similar and the differences found cannot be easily related to the treatments the samples have been submitted to.

3.3. TEM images

The evolution of the particle morphology was studied by transmission electron microscopy. The TEM images for some of the samples prepared are displayed in Fig. 2. It can be observed that in the fresh sample, a-CA0, thin particles without a defined shape are obtained. Upon 30 min of microwave-hydrothermal treatment at 125°C , sample a-CA30, a homogeneous particle size distribution of hexagonal plate-like particles is perfectly distinguished; further heating, up to 180 or 300 min, leads to larger particles either at 100 or 125°C . It should be noted that in these images it is possible to detect not only the hexagonal platelets, but also the stacking of the platelets. The shape and average dimensions of the particles aged for 180 or 300 min under microwave radiation are similar to those of a sample aged conventionally for 24 h, sample a-CAC, also shown in this figure. In some of the micrographs, the hexagonal shape of the crystallites can be readily distinguished, with an average diameter close to 100–120 nm. As some of the particles are oriented with their main plane parallel to the observation direction, also the width of the particles can be roughly measured in some cases. Such a width is close to 20–30 nm. From the thickness of a single “sandwich” (ca. 7.8 Å, as measured from the centre of a brucite-like layer to the centre of the nearest one, and corresponding to one-third of lattice parameter c) each particle should correspond to stacking of 25–40 elemental layers.

3.4. Vis–UV/DR

In order to study the eventual oxidation process of the Co^{2+} cations along the hydrothermal treatments the samples have been submitted to, the UV–Vis/DR spectra were recorded, Fig. 3. For comparison purposes, the spectra of $\text{Co}(\text{NO}_3)_2 \cdot 6\text{H}_2\text{O}$, where Co is in the divalent state and octahedrally coordinated, and Co_3O_4 , which can be also written as $\text{Co}^{\text{II}}\text{Co}_2^{\text{III}}\text{O}_4$, are included Fig. 4; while cobalt nitrate shows a light pink colour, the spinel is almost completely black. It should be noted that the spectra are rather complex because of overlapping of bands due to several species.

The spectra of all samples show a similar pattern, although some differences from one series to another can be seen, and some differences originated by the microwave irradiation treatment can be also concluded.

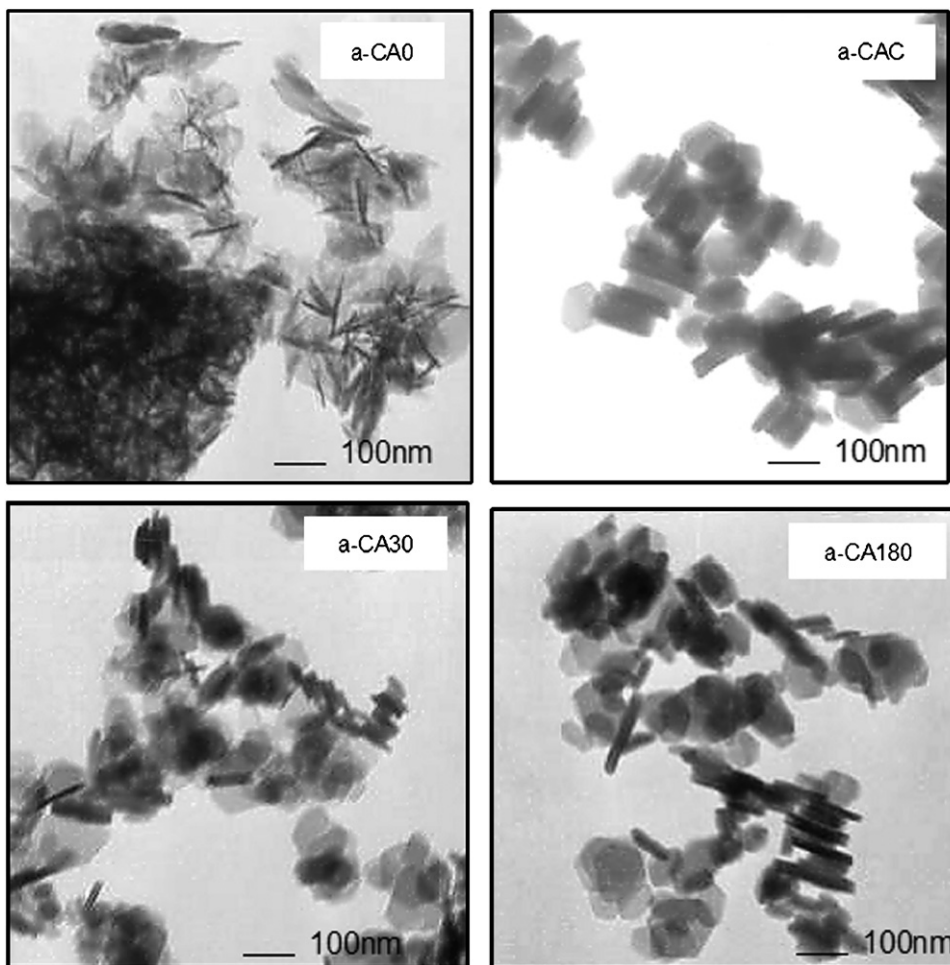


Fig. 2. Transmission electron micrographs of some representative samples: a-CA0, a-CAC, a-CA30, a-CA180.

The pink colour displayed by series a-CA samples suggests that in these samples the Co ions have not undergone any oxidation process and they exist as Co^{II} species in the octahedral holes of the brucite-like layers. An increasing absorption is recorded at large wavelengths, although, unfortunately, the maximum absorption is outside the range of the recording instrument, but it undoubtedly is above 1050–1100 nm in all cases. In addition, a multiple band, with at least three components, is also recorded in all cases. From the energy states diagram for Co^{II} ions (d^7) in an octahedral coordination, and from comparison with the spectra of $[\text{Co}(\text{H}_2\text{O})_6]^{2+}$ species—which should be very similar to those of the samples here studied—it should be concluded that the band in the near IR above 1050 nm should be due to ${}^4\text{T}_{2g}(\text{F}) \leftarrow {}^4\text{T}_{1g}(\text{F})$ transition, ν_1 ; the multiple-structure band recorded in the visible region near 525 nm, ν_3 , assigned to ${}^4\text{T}_{2g}(\text{P}) \leftarrow {}^4\text{T}_{1g}(\text{F})$; finally, transition ${}^4\text{A}_{2g}(\text{F}) \leftarrow {}^4\text{T}_{1g}(\text{F})$, ν_2 , should be responsible for the shoulder close to 620 nm, clearly detected also in the spectra of all series a-CA samples. Parameters B and Dq have been calculated from the energies corresponding to transitions ν_2 and ν_3 , using the formulae $Dq_0 = [(85\nu_3^2 - 4(\nu_3 - 2\nu_2)^2)^{1/2} - 9(\nu_3 - 2\nu_2)]/340$

and $B = (\nu_3 - 2\nu_2 + 30Dq_0)/15$; the values obtained are around 845 and 8510 cm^{-1} for all samples, leading to a value of 10 for the Δ_0/B ratio. The spectra can be analysed more precisely from the second derivative (not included), which makes clearer the multicomposed band in the middle of the visible range, around 500–600 nm. These bands can be related to spin-forbidden transitions to ${}^2\text{A}_{1g}$ and ${}^2\text{A}_{2g}$ states [39]; although their intensities should be rather low, they have been undoubtedly identified in the spectrum of $[\text{Co}(\text{H}_2\text{O})_6]^{2+}$ species [40]. Alternatively, this band can be splitted because of spin-orbit coupling, vibrational or low symmetry components, so making rather difficult a more precise analysis of the spectra [41]. It should be noted that there are no important differences in the relative intensities of the bands, nor in the intensity of the background in all these spectra, and differences cannot be either noticed between samples prepared at 100 or 125 °C.

Samples belonging to series b-CA, prepared at a higher pH, show a slightly darker colour, between light pink (as series a-CA samples) and brown, suggesting a partial oxidation of Co^{II} to Co^{III} species [21] and probably formation of the spinel, although this has not been identified by PXRD. The spectra for these samples are, in

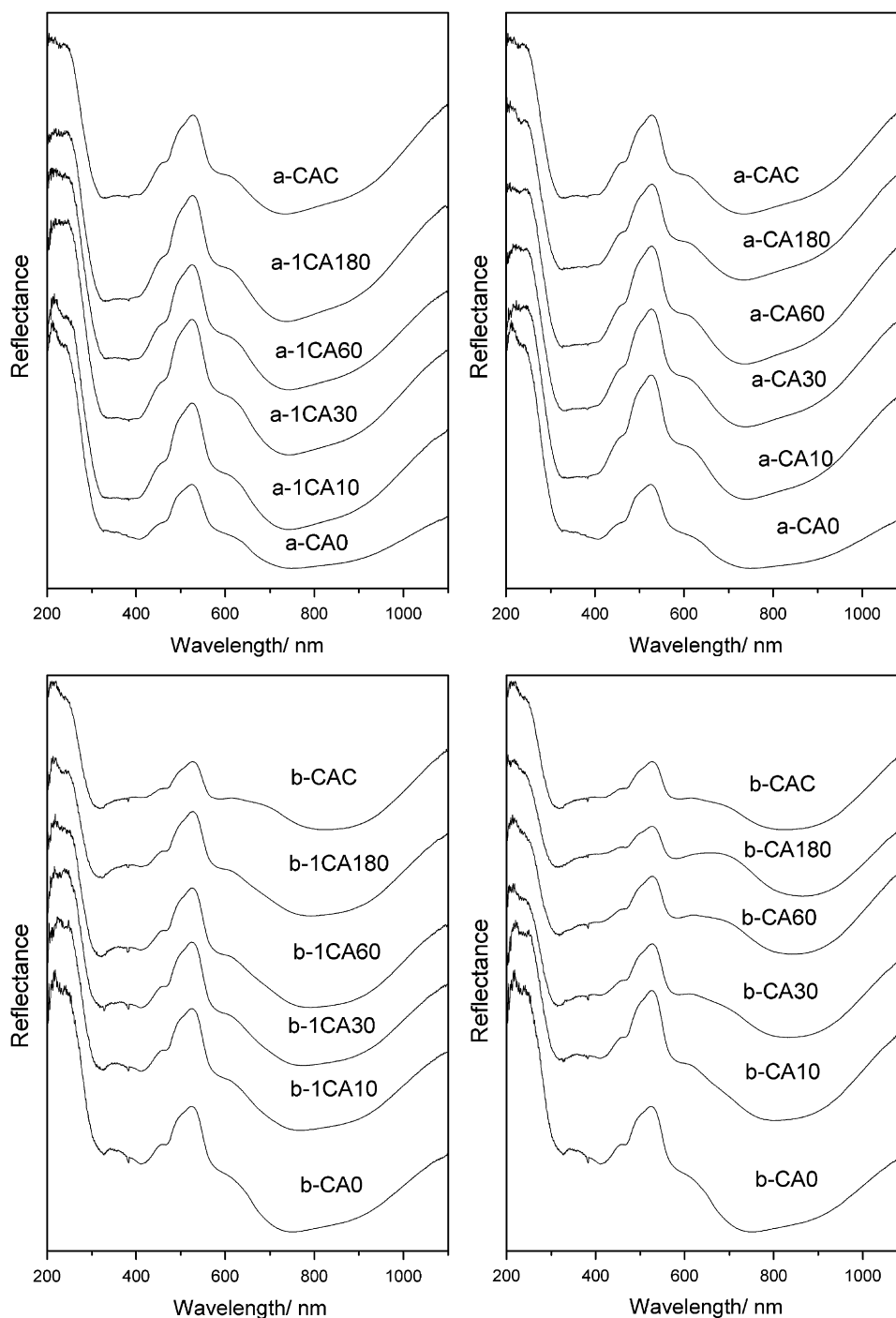


Fig. 3. Vis-UV/diffuse reflectance of the samples studied. The patterns have been vertically displaced for clarity.

some sense, similar to those of series a-CA samples, with the increased absorption at large wavelengths and the three-component band centred around 525 nm. However, the absorption between 600 and 700 nm is stronger than for series a-CA samples, at least in some of series b-CA, suggesting development of a new band which could be ascribed to $d-d$ transitions in low spin, octahedrally coordinated Co^{III} species, ${}^1\text{T}_{1g}(\text{I}) \leftarrow {}^1\text{A}_g(\text{I})$, as a result of a partial oxidation of the Co^{II} species, clearly seen from the darkening of the samples. On looking at the

shorter wavelength range, a very weak absorption close to 350 nm is also recorded in some cases, which could be tentatively ascribed to ${}^1\text{T}_{2g}(\text{I}) \leftarrow {}^1\text{A}_g(\text{I})$ transition in octahedrally coordinated Co^{III} species. The broad absorption around 600–700 nm is more evident for sample b-CAC, aged under conventional hydrothermal conditions, and it is further much more evident in the spectra of samples treated at 125 °C than in those treated at 100 °C under microwave irradiation. On the contrary, this broad feature is not observed for the untreated sample, b-CA0,

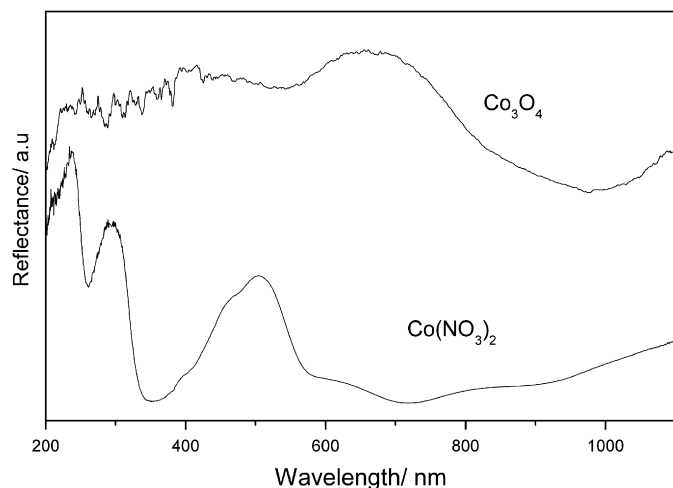


Fig. 4. Vis–UV/diffuse reflectance of the $\text{Co}(\text{NO}_3)_2 \cdot 6\text{H}_2\text{O}$ and the Co_3O_4 spinel used as references.

and so we should conclude that the oxidation process occurs during the ageing treatment, despite the confined volume of the reactor, as the $\text{Co}^{2+} \rightarrow \text{Co}^{3+}$ oxidation is thermodynamically favoured at low oxygen pressure [42]. Such an oxidation has been already reported for samples aged under hydrothermal conditions [21] and in samples with a large cobalt content [29].

Some authors have proposed that the oxidation process implies the formation of Co_3O_4 [21], while others claim [43] that it leads to structural changes, removing Al^{3+} from the layers to form octahedral polyhedra that are not washed out from the structure, demonstrating that they must be anchored or strongly bonded to the inorganic layers. The presence of these new bands in the UV–Vis spectra depends on the synthesis pH and ageing treatment, both temperature and irradiation time; for short times and low ageing temperature, only a small shoulder is observed, but when the temperature is raised up to 125 °C the band is very well evidenced.

Although undoubtedly a portion of Co^{II} ions is oxidized to the trivalent in some samples, from the Vis–UV/DR spectra we cannot conclude if the Co_3O_4 phase is actually formed in the solids synthesized (at least, its presence has not been concluded from XRD results discussed above), since the bands attributed to Co^{2+} in tetrahedral holes [42] are very close to the bands of Co^{2+} in octahedral holes and they can be overlapped.

3.5. Thermal analysis

The thermal stability of Co,Al hydrotalcites has been previously studied [43,44], showing that the decomposition mechanism of these materials differs greatly from that of other layered double hydroxides [45]. The DTA curves, recorded in air and in nitrogen, are completely different, Fig. 5. When the analyses are carried out in air all the curves show an intense single endothermic effect. This peak is due to the loss of interlayer water molecules. Unfortun-

nately, we could not analyse the nature of the gases evolved during the thermal decomposition. This behaviour (i.e., a single endothermic effect) is fairly similar to that observed for LDHs containing Al^{3+} and Li^+ cations in the layers [46,47], where decomposition takes place in a single step, including dehydration, dehydroxylation of the brucite-like layers (forming water vapour) and decarbonation from interlayer carbonate anions, leading to evolution of CO_2 . In some cases, a small exothermic peak at 300 °C has been ascribed to an oxidation process [21,28]; since this process occurs simultaneously with the thermolysis of the solid and carbonate and hydroxyl groups removal through endothermic processes, a mutual cancellation takes place to some extent [47], and consequently, for most of the samples the exothermic effect is not detected. The low stability of these Co-containing LDHs has been attributed to the oxidation process described above [44]. Oxidation of Co^{2+} to Co^{3+} in the presence of air may cause its diffusion to the interlayer space; simultaneous dehydroxylation of the brucite-like sheets favours the formation of O–M–O bonds between the layers, inducing the collapse of the layered structure and formation of a stable mixed oxide phase $\text{Co}(\text{Co},\text{Al})_2\text{O}_4$ at relatively low temperatures [43].

A completely different picture emerges when the analyses are carried out in N_2 . A first (weaker) endothermic peak persists in the same position as that recorded in oxygen but, in addition, a second endothermic peak is recorded. As under these experimental conditions, oxidation of Co^{2+} to Co^{3+} —giving rise to an exothermic effect—cannot take place, the second endothermic effect due to collapse of the layered structure after dehydroxylation and decarbonation is now clearly recorded at ca. 270 °C. PXRD analysis of the residue after heating in nitrogen shows formation of crystalline CoO and mostly amorphous CoAl_2O_4 .

The peaks slightly shift to higher temperatures when the MW-irradiation time is increased, indicating that in addition to an increase in the crystallinity degree, the microwave-hydrothermal treatment improves the thermal stability of the solids.

The TG curves (Fig. 5) show in all cases a first important weight loss, typically ca. 18% of the initial sample weight, which has been previously ascribed to removal of water, in agreement with the DTA results discussed above. The weight loss in the second step is ca. 20% of the initial sample weight, corresponding to removal of CO_2 (from carbonate ions) and water (from condensation of hydroxyl groups); in this last process there is a collapse of the layered structure. Total weight loss was around 38–40% for all the samples. The water content in the samples, given in Tables 1 and 2, was calculated from the weight loss of the samples recorded in nitrogen, where results indicated that the oxidation state of the cobalt is preserved.

3.6. FT-IR spectroscopy

The FT-IR spectra of the samples are similar to the spectra reported for hydrotalcite-like compounds [48]. For

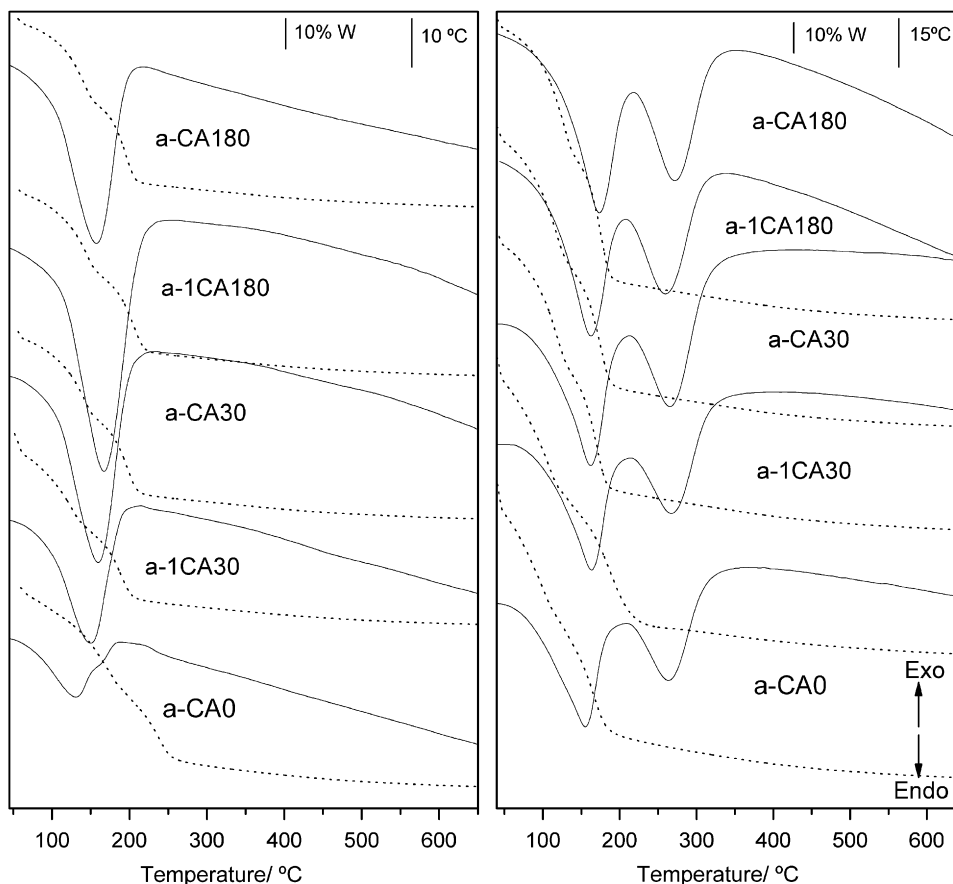


Fig. 5. Thermogravimetric (dotted line) and differential thermal analysis (solid line) of representative samples recorded in air (left) and nitrogen (right). The patterns have been vertically displaced for clarity.

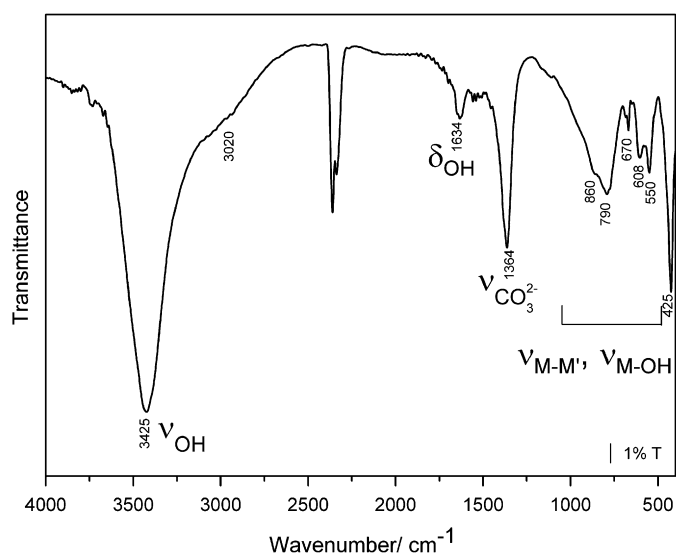


Fig. 6. FT-IR spectra of sample a-CA180.

the sake of brevity, only the spectrum of one of the samples is shown in Fig. 6, as all they are very similar to each other. The broad and intense band around 3400 cm^{-1} is due to ν_{OH} stretching mode, and the shoulder around 3050 cm^{-1} is attributed to the ν_{OH} stretching mode of water molecules

hydrogen-bonded to interlayer carbonate anions; this second band is more remarkable in the spectra of the most crystalline samples, in agreement with previous results [49,50]. The water deformation mode, δ_{HOH} , is recorded around 1630 cm^{-1} in all cases with negligible differences between one sample and another. The band due to the ν_{OH} mode, and the intense peak around 1360 cm^{-1} corresponding to the ν_3 mode of CO_3^{2-} , become narrower and more symmetric under hydrothermal treatment, whichever conventional or with microwave irradiation, such features being more evident as the irradiation time is prolonged [49]. The shoulder recorded around 860 cm^{-1} is due to the ν_2 carbonate mode, while the in-plane bending, ν_4 , is not clearly observed around $670\text{--}680\text{ cm}^{-1}$. In the low wavenumber region, the bands attributed to stretching modes of the octahedral layers are also recorded. The bands assigned to translational modes of hydroxyl groups influenced by trivalent aluminium, Al-OH translation, are recorded at 790 and 550 cm^{-1} . The peak observed around 610 cm^{-1} has been ascribed to a Co-OH translational mode [51,52]. Finally, the band around 430 cm^{-1} is due to condensed $[\text{AlO}_4]^{5-}$ groups or to Al-O simple bonds [53]. In this region, there is a change in the relative intensities of the bands around 550 and 608 cm^{-1} , this behaviour being more evident for bCA samples. The bands attributed to Co_3O_4

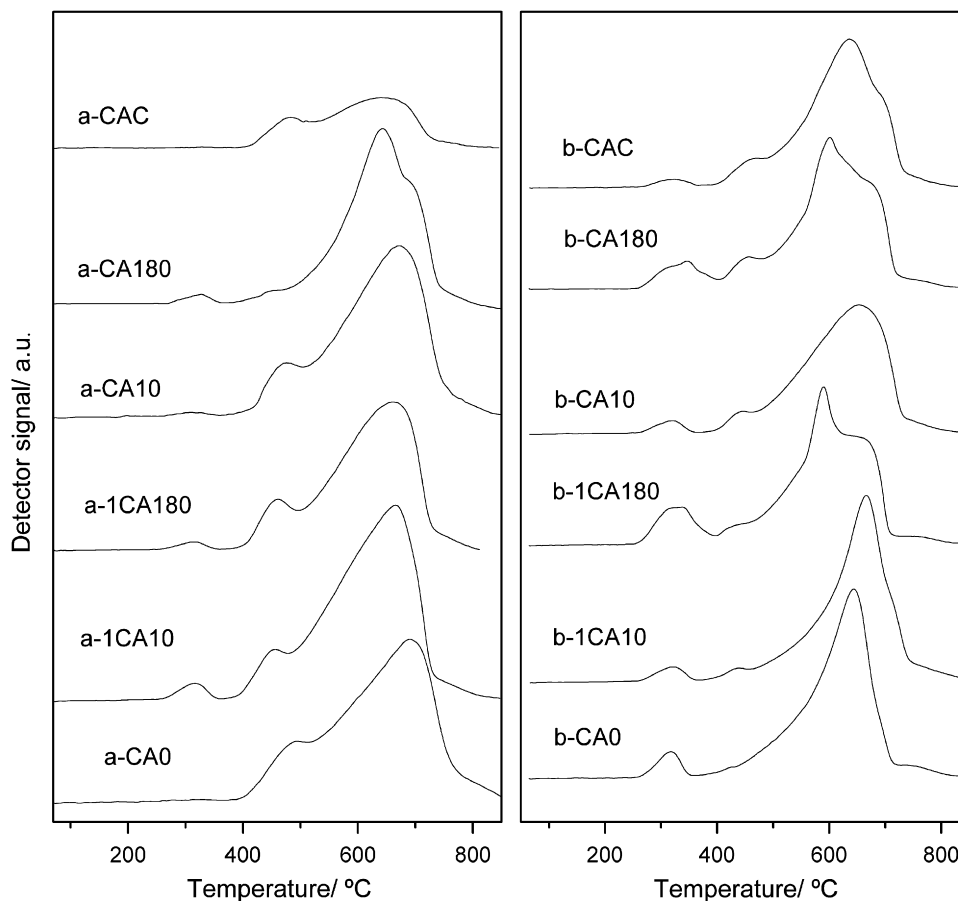


Fig. 7. Temperature-programmed reduction of some representative samples. The patterns have been vertically displaced for clarity.

are recorded at around 672 and 590 cm^{-1} , involving Co^{2+} and Co^{3+} species, respectively. It can be tentatively claimed that the increase in the intensity of the band ascribed to the Al–OH translational mode is related to the presence of a higher amount of trivalent cobalt, suggesting the formation of cobalt spinel during the treatment, although it was not detected by PXRD because well dispersed, small particles should be formed. However, it is very difficult to conclude about the band around 672 cm^{-1} , because it is quite close to the position for the ν_4 band.

3.7. Temperature-programmed reduction (TPR)

TPR was used to examine the redox properties of LDHs. Fig. 7 shows the TPR curves for some selected samples. Although Al^{3+} is not reduced under the experimental conditions used in our TPR runs, the reduction of Co^{n+} to Co^0 has been previously reported [1,54]. A first weak reduction is sometimes recorded around 300°C , but its intensity has no relationship with the ageing treatment of the samples and its origin remains obscure. Some authors have attributed it to the reduction of NO_3^- to NO [55], but in our case the FT-IR spectra show that the anion present in the hydrotalcite structure is exclusively CO_3^{2-} , and element chemical analysis gave no evidence of nitrogen

presence in the samples. Above this temperature, a single, despite composed, broad peak is recorded. The absolute maximum is recorded around 650°C , with an important shoulder around 450°C . Samples aged under conventional hydrothermal treatment show only broad peaks, indicating that reduction takes place in a broad temperature range. However, the original samples and the microwave-irradiated ones display TPR curves with sharper peaks, extending in narrower temperature ranges.

Recording several peaks in a TPR curves of cobalt-containing (or other reducible cations) samples might be originated, at least, by two different situations: (i) a stepwise reduction of the cobalt cations, e.g., $\text{Co}^{3+} \rightarrow \text{Co}^{2+}$ and $\text{Co}^{2+} \rightarrow \text{Co}^0$, or (ii) reduction in a single step ($\text{Co}^{3+} \rightarrow \text{Co}^0$ or $\text{Co}^{2+} \rightarrow \text{Co}^0$) of species with different morphologies or particles with different shape or size. Moreover, as the structure is being modified along the heating process, while the cations are being reduced, a fine-tuned analysis of the reduction process is extremely difficult, much more than reduction, for instance, of oxides which do not undergo any structure modification, but reduction, during heating.

The area under the curve is directly related to H_2 consumption during the reduction, and thus, from a knowledge of the amount of reducible cations (Co^{2+} in our

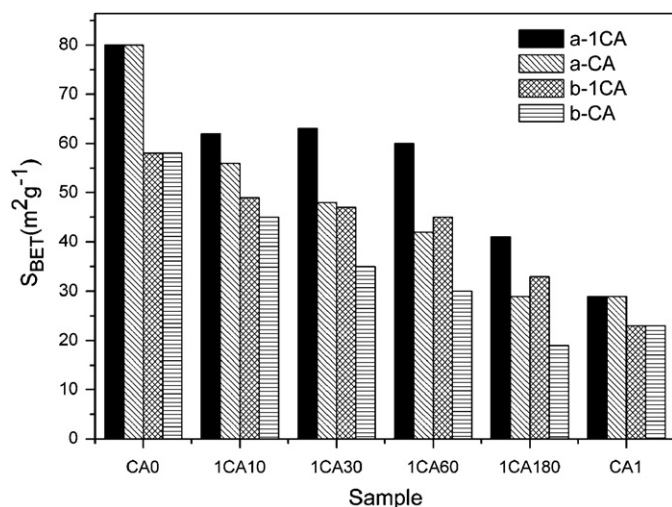
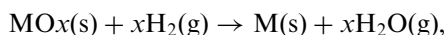


Fig. 8. Change in the specific surface area of the different series of samples studied.

case) and the amount of hydrogen consumed, the original oxidation state of the cation can be determined, according to the process:



as such a reduction to the zero-valent state of cobalt is thermodynamically favourable under the reaction conditions used. If all cobalt species are in the divalent state in the unreduced sample, the expected value for the H₂/Co molar ratio is 1.00, while such a ratio reaches a value of 1.33 for reduction of Co₃O₄, or 1.50 for Co³⁺ species. The values measured for series a samples were 1.06 ± 0.2, suggesting that the average oxidation state of cobalt ions in these samples is 2.0, in agreement with the pink colour of these samples, characteristic of Co²⁺ cations in an octahedral coordination of oxide or hydroxyl anions. However, the values for samples belonging to series b were closer to 1.3–1.4, indicating that a fraction of the Co²⁺ cations have become oxidized to the trivalent state during their preparation. Consequently, the samples display a brown colour, and the Vis–UV spectrum corresponds to the simultaneous presence of Co²⁺ and Co³⁺ species.

3.8. Surface area measurement

The specific surface areas were calculated by the well-known B.E.T. method from the nitrogen adsorption isotherms recorded at –196 °C. All samples displayed type II nitrogen adsorption isotherms, according to the IUPAC classification [56]. These indicate that all samples are either mesoporous or non-porous, without micropores, i.e., nitrogen molecules are unable to penetrate in the interlayer space of these materials with rather small interlayer anions [1]. As expected [57], the specific surface area values change with the ageing treatment to which the samples had been submitted. A decrease in the values is observed, Fig. 8,

when the samples are aged under the influence of microwave radiation. However, in both series, the specific surface area of samples irradiated for 180 min, when the samples are heated at 100 °C, is larger than that measured for the sample aged by the conventional treatment. This behaviour can be tentatively explained by an increased formation and growth of mesopores [58], but a more precise explanation is still lacking.

4. Conclusions

Layered double hydroxides with cobalt and aluminium cations in the brucite-like layers, and with carbonate in the interlayer have been prepared. A precise control of pH during precipitation stabilizes cobalt species in the divalent state, as concluded from the results obtained mainly by Vis–UV spectroscopy and TPR. Thermal decomposition in nitrogen cancels oxidation to Co³⁺ species, which is, however, observed if the analysis is carried out in oxygen or air.

Acknowledgments

Authors thank financial support from MCyT (Grant MAT2003-06605-C02-01), Fundación Samuel Solorzano and JCyL (Grant SA030/03), ERDF, CONCORDE and to Mr. A. Montero for his assistance in obtaining some of the experimental results. P.B. acknowledges a grant from JCyL.

References

- [1] V. Rives (Ed.), Layered Double Hydroxides: Present and Future, Nova Science Publishers, New York, 2001.
- [2] F. Wypych, K.G. Satyanarayana (Eds.), Clay Surfaces: Fundamentals and Applications, Elsevier Academic Press, London, 2004.
- [3] X. Duan, D.G. Evans, Struct. Bond. 119 (2006).
- [4] A.S. Bookin, V.A. Drits, Clays Clay Miner. 41 (1993) 551–557.
- [5] V. Rives, M.A. Ulibarri, Coordin. Chem. Rev. 181 (1999) 61–120.
- [6] S.P. Newman, W. Jones, N. J. Chem. 22 (1998) 649–649.
- [7] G. Fornasari, S. Gusi, F. Trifiró, A. Vaccari, Ind. Eng. Chem. Res. 26 (1987) 1500–1505.
- [8] A.A. Khassin, T.M. Yurieva, G.N. Kustova, I.S. Itenberg, M.P. Demeshkina, T.A. Krieger, L.M. Plyasova, G.K. Chermashentseva, V.N. Parmon, J. Mol. Catal. A 168 (2001) 193–207.
- [9] S. Kannan, C.S. Swamy, Appl. Catal. B 3 (1994) 109–116.
- [10] J.N. Armor, T.A. Braymer, T.S. Farris, Y. Li, F.P. Petrocelli, E.L. Weist, S. Kannan, C.S. Swamy, Appl. Catal. B 7 (1996) 397–406.
- [11] S. Kannan, Appl. Clay Sci. 13 (1998) 347–362.
- [12] S. Kannan, C.S. Swamy, Catal. Today 53 (1999) 725–737.
- [13] J. Pérez-Ramírez, J. Overijnder, F. Kapteijn, J.A. Moulijn, Appl. Catal. B 23 (1999) 59–72.
- [14] R. Unnikrishnan, S. Narayanan, J. Mol. Catal. A 144 (1999) 173–179.
- [15] A.E. Palomares, J.M. López-Nieto, F.J. Lázaro, A. López, A. Corma, Appl. Catal. B 20 (1999) 257–266.
- [16] S.R. Segal, K.B. Anderson, K.A. Carrado, C.L. Marshall, Appl. Catal. A 231 (2002) 215–223.
- [17] V. Rives, O. Prieto, A. Dubey, S. Kannan, J. Catal. 220 (2003) 161–171.
- [18] V. Rives, A. Dubey, S. Kannan, Phys. Chem. Chem. Phys. 3 (2001) 4826–4836.

- [19] D. Zhao, C.H. Liu, L.Q. Wang, S.C. Zhang, *Chin. J. Catal.* 24 (2003) 595–599.
- [20] S. Kannan, C.S. Swamy, *J. Mater. Sci. Lett.* 11 (1992) 1585–1587.
- [21] M.A. Ulibarri, J.M. Fernández, F.M. Labajos, V. Rives, *Chem. Mater.* 3 (1991) 626–630.
- [22] S. Kannan, S. Velu, V. Ramkumar, C.S. Swamy, *J. Mater. Sci.* 30 (1995) 1462–1468.
- [23] S. Kannan, C.S. Swamy, Preparation of catalysts VI, in: G. Poncelet, et al. (Eds.), *Scientific Bases for the Preparation of Heterogeneous Catalysts*, Elsevier Science B. V., Amsterdam, 1995, pp. 903–914.
- [24] S. Kannan, C.S. Swamy, *J. Mater. Sci.* 32 (1997) 1623–1630.
- [25] M. Del Arco, R. Trujillano, V. Rives, *J. Mater. Chem.* 8 (1998) 761–767.
- [26] X.P. Xu, H.C. Zeng, *J. Mater. Chem.* 8 (1998) 2499–2506.
- [27] X.P. Xu, H.C. Zeng, *Chem. Mater.* 11 (1999) 67–74.
- [28] X.P. Xu, H.C. Zeng, *Chem. Mater.* 12 (2000) 3459–3465.
- [29] F. Leroux, E. Moujahid, C. Taviot-Gueho, J.P. Besse, *Solid State Sci.* 3 (2001) 81–92.
- [30] B. Zapata, P. Bosch, G. Fetter, M.A. Valenzuela, J. Navarrete, V.H. Lara, *Int. J. Inorg. Mater.* 3 (2001) 23–29.
- [31] D.A. Jones, T.P. Lelyveld, S.D. Mavrofidis, S.W. Kingman, N.J. Miles, *Resourc. Conserv. Recycling* 34 (2002) 75–90.
- [32] W.T. Reichle, *Solid State Ion.* 22 (1986) 135–141.
- [33] JCPDS: Joint Committee on Powder Diffraction Standards, International Centre for Diffraction Data, Pennsylvania, USA, 1977.
- [34] P. Malet, J. Caballero, *J. Chem. Soc. Faraday Trans.* 84 (1988) 2369–2375.
- [35] V. Rives, *Adsorpt. Sci. Technol.* 8 (1991) 241–251.
- [36] J.M. Fernández, C. Barriga, M.A. Ulibarri, F.M. Labajos, V. Rives, *Chem. Mater.* 9 (1997) 312–318.
- [37] H.C. Zeng, Z.P. Xu, M. Qian, *Chem. Mater.* 10 (1998) 2277–2283.
- [38] F. Trifirò, A. Vaccari, O. Clause, *Catal. Today* 21 (1994) 185–195.
- [39] A.B.P. Lever, in: *Inorganic Electronic Spectroscopy*, Elsevier, New York, 1984.
- [40] K.D. Gailey, R.A. Palmer, *Chem. Phys. Lett.* 13 (1972) 176–180.
- [41] D. Sutton, *Espectros electrónicos de los complejos de los metales de transición*, Ed. Reverté, 1975.
- [42] J. Pérez-Ramírez, G. Mul, F. Kapteijn, J.A. Moulijn, *Mater. Res. Bull.* 36 (2001) 1767–1775.
- [43] J. Pérez-Ramírez, G. Mul, F. Kapteijn, J.A. Moulijn, *J. Mater. Chem.* 11 (2001) 821–830.
- [44] J. Pérez-Ramírez, G. Mul, J.A. Moulijn, *Vib. Spectrosc.* 27 (2001) 75–88.
- [45] J.M. Hernández, M.A. Ulibarri, J. Cornejo, M.J. Peña, J.C. Serna, *Thermochim. Acta* 94 (1985) 257–266.
- [46] G. Mascolo, *Thermochim. Acta* 102 (1986) 67–73.
- [47] E. Uzunova, D. Klissurski, I. Mitov, P. Stefanov, *Chem. Mater.* 5 (1993) 576–582.
- [48] J.T. Klopogge, in: J.T. Klopogge (Ed.), *The Application of Vibrational Spectroscopy to Clay Minerals and Layered Double Hydroxides*, CMS Workshop Lectures, vol. 13, The Clay Mineral Society, Aurora, CO, 2005, p. 203.
- [49] S. Kannan, S. Velu, V. Ramkumar, C.S. Swamy, *J. Mater. Sci.* 30 (1995) 1462.
- [50] P. Benito, F.M. Labajos, V. Rives, *Bol. Soc. Esp. Ceram. y Vidrio* 43 (2004) 56–58.
- [51] J.T. Klopogge, R.L. Frost, *J. Solid State Chem.* 146 (1999) 506–515.
- [52] J.T. Klopogge, R.L. Frost, *Appl. Catal. A* 184 (1999) 61–71.
- [53] M.L. Valchevatraykova, N.P. Davidova, A.H. Weiss, *J. Mater. Sci.* 28 (1993) 2157–2162.
- [54] V. Rives, M.A. Ulibarri, A. Montero, *Appl. Clay Sci.* 10 (1995) 83–93.
- [55] O. Lebedeva, D. Tichit, B. Coq, *Appl. Catal. A* 183 (1999) 61–71.
- [56] K.S.W. Sing, D.H. Everett, R.A.W. Haul, L. Moscou, R. Pierotti, J. Rouquerol, T. Sieminska, *Pure Appl. Chem.* 57 (1985) 603–619.
- [57] F.M. Labajos, V. Rives, M.A. Ulibarri, *J. Mater. Sci.* 27 (1992) 1546–1552.
- [58] S. Kannan, R.V. Jasra, *J. Mater. Chem.* 10 (2000) 2311–2314.